Available online at www.sciencedirect.com

ScienceDirect

journal homepage: www.jfda-online.com

Original Article

rGO-NS SERS-based coupled chemometric prediction of acetamiprid residue in green tea

Md Mehedi Hassan, Quansheng Chen, Felix Y.H. Kutsanedzie, Huanhuan Li, Muhammad Zareef, Yi Xu, Mingxiu Yang, Akwasi A. Agyekum*

School of Food and Biological Engineering, Jiangsu University, Zhenjiang 212013, PR China

ARTICLE INFO

Article history:
Received 3 May 2018
Received in revised form
14 June 2018
Accepted 19 June 2018
Available online 4 July 2018

Keywords:
Acetamiprid residue
Chemometrics
Green tea
Reduced graphene oxide-gold nanostar
Surface-enhanced Raman scattering

ABSTRACT

Pesticide residue in food is of grave concern in recent years. In this paper, a rapid, sensitive, SERS (Surface-enhanced Raman scattering) active reduced-graphene-oxide-gold-nano-star (rGO-NS) nano-composite nanosensor was developed for the detection of acetamiprid (AC) residue in green tea. Different concentrations of AC combined with rGO-NS nano-composite electro-statically, yielded a strong SERS signal linearly with increasing concentration of AC ranging from 1.0×10^{-4} to 1.0×10^{3} μg/mL indicating the potential of rGO-NS nano-composite to detect AC in green tea. Genetic algorithm-partial least squares regression (GA-PLS) algorithm was used to develop a quantitative model for AC residue prediction. The GA-PLS model achieved a correlation coefficient (Rc) of 0.9772 and recovery of the real sample of 97.06%–115.88% and RSD of 5.98% using the developed method. The overall results demonstrated that Raman spectroscopy combined with SERS active rGO-NS nano-composite could be utilized to determine AC residue in green tea to achieve quality and safety.

1. Introduction

Green tea, *Camellia sinensis (L.)*, is one of the most popular drinks consumed daily by millions of people around the world due to its colossal medicinal properties. Many researchers have suggested that polyphenols of green tea possess anti-oxidant activities which play a significant role in the prevention of cardiovascular disease, chronic gastritis and some cancers including skin, breast, prostate, colorectal, liver and lung etc. [1,2]. To meet the growing demand of tea across the world, growers employ pesticides to increase production and curb the ravaging effects of pest and diseases. AC is abroad spectrum neonicotinoid insecticide widely used to control sucking and chewing pest. It easily combines with nicotinic acetylcholine receptors (nAChRs, a signal receptor in the neuron) of the pest to cause paralysis or death [3]. However, neonicotinoid insecticide slightly toxic to mammals especially human. α4β2 nAChR is a subtype of nAChR; AC can directly activate and modulate human α4β2 nAChR by altering the

* *Corresponding author*. Fax. +86 511 88780201.
E-mail address: qschen@ujs.edu.cn (Q. Chen).

https://doi.org/10.1016/j.jfda.2018.06.004

receptor density resulting in Central Nervous System (CNS) disorders such as Alzheimer's disease, Parkinson's disease, schizophrenia, and depression [4]. Different analytical methods including HPLC (high performance liquid chromatography) [5], LC-MS-MS (Liquid chromatography–tandem mass spectrometry) [6], ELISA (enzyme-linked immune sorbent assays) [7], fluorescent assays [8] have been used for the analysis of pesticide residues such as AC in various food matrices. Although these methods show high accuracy, precision and selectivity, they have some limitations in the practical application including complicated sample preparation procedure, high skilled labour for system operation, time-consuming, and cost-intensive as well. Therefore, there is high demand for the development of a label-free, simple, sensitive and economical method for the trace detection of AC.

Vibrational spectroscopic methods, such as Raman spectroscopy, as one of the most sensitive detection technologies, has been used for the identification contaminants and residues in food such as pesticides [9], heavy metals [10], toxins [11], antibiotics [12] and biogenic amine [13] etc. This is mainly due to the surface plasmon of the noble metal nanostructure surface [such as silver and gold] that gives a strong Raman enhancement signal which represents "fingerprint-like" information about various chemicals [14]. Zheng (2017) described the two mechanisms of SERS occurrence: electromagnetic mechanism (EM) which is based on the enhancement of the local electromagnetic field incident on absorbed molecules at the metallic nanostructures; and chemical mechanism (CM) on the other hand which is highly dependent on the electronic resonance-charge transfer effect between adsorbed molecules and metal surface roughness features [15]. Recently several studies have been reported on SERS based rapid detection of AC and most of them were focused on fruits and juice using gold or silver nano-particle; albeit, silver has 10 to 100 times higher SERS enhancement than gold but silver nanoparticle can be easily oxidized than gold when exposed to air [9,16]. Under same experimental conditions, gold nano-stars exhibits stronger SERS enhancement than a nano-rods and nano-spheres [17]. Graphene, a single-atom, two-dimensional sheet of a hexagonal carbon atom, has attracted increasing attention in recent times due to its efficiency for SERS since its discovery in 2004 by Geim and co-workers [18,19]. Citrate mediated reduction of GO with Au yielded spherical nanoparticles which are less efficient for SERS application due to the less surface roughness of gold nanoparticles; whereas seed mediated synthesis of rGO-NS provided more rough surfaces to create 'hot spots' which aided more intense Raman signal enhancement, making them more effective for SERS sensing application. Reduced Graphene oxides (rGO) can protect the nano-stars from aggregation, enhance the SERS efficiency as well as bring the aromatic molecules closer to the nano-stars surface. However, without using any surfactant or polymer stabilizers reduced graphene oxide (rGO) can control the morphology of rGO-NS nano-hybrids and the corresponding optical properties [20].

Multivariate calibration methods (PCA, PLS, GA-PLS) are widely used for spectrum information analysis and building of calibration models for quantitative and qualitative determination of analytes from a sample [21–23]. Partial least square (PLS) is one of the most commonly multivariate statistical regression tools that work on a full spectrum and preserves all the information collected from the samples [24]. PLS models are built using full spectra obtained from samples and therefore contain irrelevant information and which affects the prediction stability of their built models [25–27]. On the contrary, GA-PLS is a variable selection algorithm, which can be used to remove or reduce the irrelevant and collinear spectral variable contained in the acquired spectra to improve the model prediction stability and robustness [27].

Albeit, tea has many medicinal properties, and largely consumed because of its manifold health benefits, their contamination from spraying of pesticides results in the converse. In order to safeguard the quality and safety levels of these pesticides contaminants in tea, a rapid method is needed. Thus, this study is therefore geared towards the fabrication of SERS based nanosensors to provide antidote to the hitherto conventional techniques which are reportedly cumbersome in operation, time-consuming and chemical dependent. The success of this study is expected to be deployed to the boost safety and quality levels of tea to protect the consumers' health and businesses of producers.

The objective of this study was to use SERS based seed-mediated synthesized gold nano-stars (AuNS) supported on reduced graphene oxide (rGO) coupled to the genetic algorithm-partial least square algorithm (GA-PLS) for the rapid detection of AC insecticide residue extracted from green tea. Seed-mediated growth method can be synthesized AuNS on top of the rGO surface as a controllable way. An illustration of the detection process is shown in Schematic diagram 1.

2. Materials and methods

2.1. Regents

Graphene oxide stock solution (2 mg/mL) was purchased from Tanfeng Tech. Inc. (Suzhou, China). Acetamiprid (98.3%) was purchased from Shanghai Pesticide Research Institute Co., Ltd. (Shanghai, China). Chloroauric acid tetrahydrate ($HAuCl_4 \cdot 4H_2O$, ≥99.5%), tri-sodium citrate dihydrate ($C_6H_5Na_3O_7 \cdot 2H_2O$, ≥99.0%), crystal violet (CV) hydrochloric acid solution (37%), silver nitrate (AgNO3, ≥99.0%) and L-ascorbic acid (AA, ≥ 99%) (analytical grade) were obtained from Sinopharm Chemical Reagent Co. Ltd. (Shanghai, China). All chemicals were used without further purification. Ultrapure Milli-Q water was used throughout the experiments.

2.2. Instrumentation

Ultraviolet–visible (UV–vis) absorption spectrum was measured using a UV–vis spectroscopy (Agilent Technologies Inc). A transmission electron microscope (JEM-2100HR; TEM, JEOL Ltd., Japan) was used to detect the size and morphology of nano-composite. S–3400N scanning electron microscope (SEM, Hitachi Ltd., Japan) was used for capturing the structure of nano-composite whiles energy dispersive spectroscopy (EDS) (Hitachi Ltd., Japan) was used for elemental analysis. X-ray diffraction (XRD) pattern was obtained by D8-advance instrument (Bruker AXS Ltd., Germany). The Zeta potential

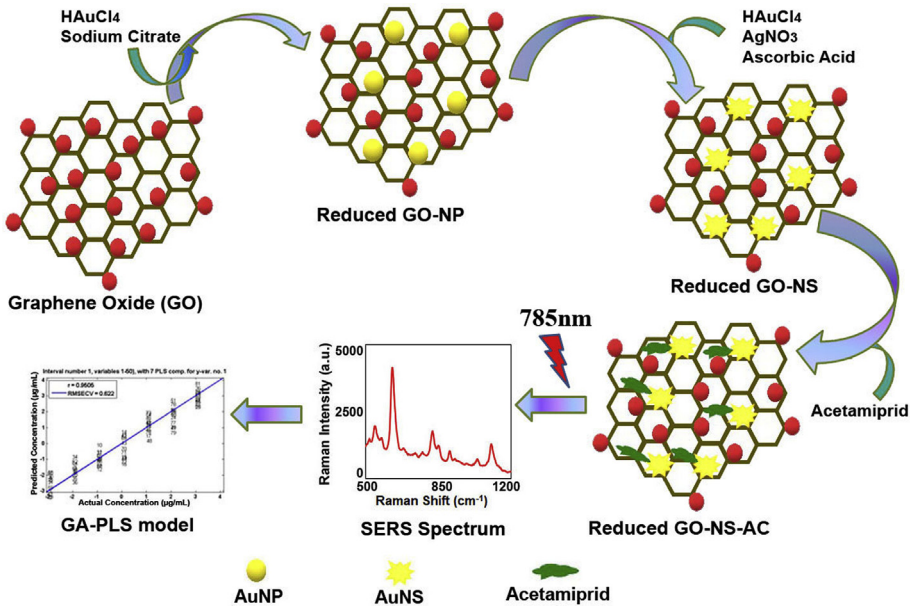

Schematic diagram 1 – Schematic illustration of the synthesis of gold nano-stars (AuNS) supported on reduced graphene oxide (rGO) for AC detection by SERS.

measurements were performed by the Nano-ZS Zetzsozer ZEN3600 (Malvern Instruments Ltd., UK). FT-IR (Fourier transform infrared) spectra were recorded using a Nicolet Nexus 470 Fourier transform infrared spectrophotometer (Thermo Electron Co.). Raman spectra were collected using an SPLD-RAMAN-785-Q Spectrometer (Hangzhou SPL photonics Co Ltd., China) with 785 nm wavelength incident laser light.

2.3. *Synthesis of reduced graphene Oxide-Au nanoparticle (rGO-NP) nano-composites and reduced graphene Oxide-Au nanostar (rGO-NS) nano-composites*

The rGO-NP nano-composites and rGO-NS nano-composites were prepared by a modified method of Wang et al., 2014 [20]. Briefly, 0.4 mL of 2 mg/mL graphene oxide aqueous suspension was diluted with 10 mL water and sonicated for 30 min at 25 °C temperature. Then 98 μL of 25 mM $HAuCl_4$ was added and stirred for 30 min. After that, the solution was heated up to ~85 °C, and 100 μL of 1.0 M sodium citrate was added dropwise under continuous stirring under the stated conditions for 60 min. Finally, the reaction mixture was stored for more than 1 h to form rGO-NP colloidal solution. Reduced graphene oxide (rGO) solution was prepared by following the above procedure devoid of $HAuCl_4$.

For the synthesis of rGO-NS nano-composite, 0.2 mL as prepared rGO-NP seed solution (AuNP, ~10.0 nm average diameter, on rGO surface, see Fig. S1 in the Supporting Information for TEM images) was added to 20 mL of 0.25 mM $HAuCl_4$ solution, followed by the addition of 10 μL of 1 M HCl under moderate stirring. 200 μL of 2 mM silver nitrate and 100 μL of 0.1 M ascorbic acid (AA) were added quickly to the above mixture. The solution was stirred for 30 s, until the solution changed from light red to blue, signalling the completion of the process see Fig. 1e.

2.4. *SERS spectrum measurement for AC*

1000 μg/mL standard stock solution of AC was prepared from a standard chemical of AC using 5% (v/v) ethanol. Working solutions of 0.0001, 0.001, 0.01, 0.1, 1, 10, 100 and 1000 μg/mL of AC were prepared by serial dilutions from 1000 μg/mL of AC and added to green tea sample. AC residue was extracted from green tea by the procedure of Ru-Yan et al., 2013 (See in Supporting information) and twenty samples were prepared for each concentration. Green tea (Longjing tea leaves) was purchased in a sealed plastic pack from the local Auchan supermarket and stored under refrigeration condition at 4 °C. The colloidal solution of rGO-NS nano-composite was dropped on the 0.8 × 0.8 mm silicon wafer and dried at room temperature. The SERS spectrum was collected from the AC loaded SERS substrate complex formed on the silicon plate. Three spectra were collected from each sample at three different spots and then averaged to obtain the final spectrum of each sample. The Raman spectra were collected using SPLD-RAMAN-785-Q spectrometer with an excitation power of 350 mW under a 785 nm laser excitation, focused onto the sample at a microscope stage through a 50 × /0.55 objective. Each spectrum was scanned from 336 to 2000 cm^{-1} and the acquisition time was 3 s.The solvent except pesticide was used as the blank.

2.5. *Spectral processing*

In this study, standard normal variate transformation (SNV) was applied for spectral processing. SNV is a mathematical row-oriented transformation method which centres and scales individual spectrum used to remove slope variation, correct instrument noise and background interference [27,28]. The raw SERS spectra of AC comprised not only chemical-

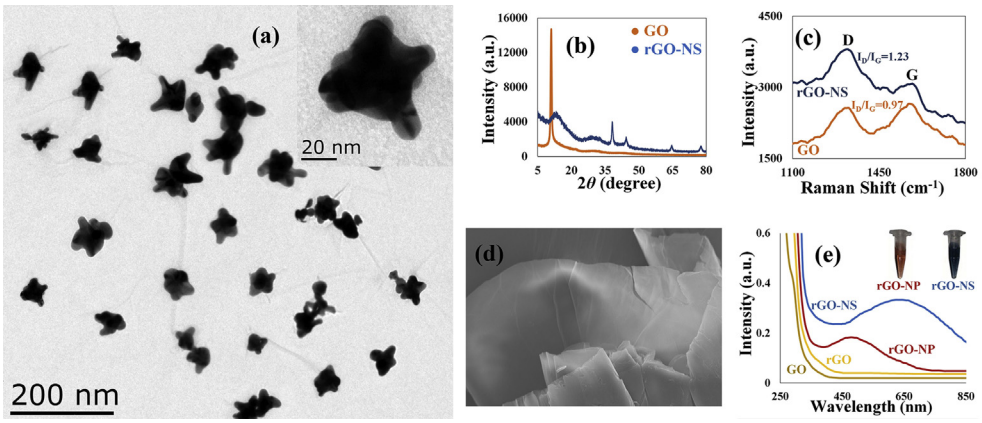

Fig. 1 – TEM image of reduced graphene oxide supported gold nano-stars (rGO-NS) and the gold nano-stars have an average size of 60.37 nm with 8 branches (on average) (a). XRD pattern of GO and rGO-NS nano-composites (b). Raman spectra depicting D and G band of GO and rGO-NS nano-composites (c). An SEM image of graphene oxide (d), UV–vis extinction spectrum of GO, rGO, rGO-NP and rGO-NS nano-composite as well as a photograph of rGO-NP and rGO-NS mentioned at the top left corner of figure (e).

related information but also retained other interference information, such as instrument noise, sample background interference and fluorescence interference, which ultimately affects the accuracy and repeatability of the measurement. However, the SNV method is able to reduce these interferences. The SNV was calculated by the equation below:

$$x_{i,SNV} = \frac{x_{i-x^-}}{\sqrt{\sum_{i=1}^{n}(x_i - x^-)^2 / (n-1)}}$$

where x_{iSNV} is the SNV transformed spectral value for i th variable, x_i is the ith variable in the raw spectrum, and x is the mean of the raw spectrum.

2.6. Chemometric analysis of AC

GA-PLS: It is significantly important to select a suitable algorithm in order to achieve a superior quantitative model for AC residue detection using SERS technology combined with the chemometric algorithm. GA-PLS is an advanced hybrid approach which was developed by the fusion of GA with a powerful optimization method PLS as an important statistical tool for variable selection. The descriptor data matrix is decomposed into orthogonal matrices by the inner relationship between dependent and independent variables during PLS analysis. A minimal number of latent variables are used for PLS modelling as the multi-co-linearity problem in the descriptors can be deleted by the PLS analysis and this model also coincides with noisy data. On the contrary, GA can effectively solve the problem of random correlations existing in the GA algorithm and multi-co-linearity among the variables [27,29]. GA consists of five components, including evaluation, selection, recombination, mutation, and reinsertion. These components are repeated until a final outcome is reached.

The performance of the developed model was evaluated according to the root mean square error of cross-validation (RMSECV), the root mean square error of prediction (RMSEP), the correlation coefficient of calibration (Rc) and the correlation coefficient of prediction (Rp) [30]. Lower RMSECV and RMSEP and higher Rc and Rp suggest that the model has better precision; additionally, the model with satisfactory robustness should have minimal differences between RMSECV and RMSEP and between Rc and Rp. Moreover, the number of principal components (PCs) should have low so that the model performance cannot be affected by the reduced computational complexity on the premise [31].

In favour of RMSECV, a cross-validation was executed by the removal one sample spectrum of the calibration set to build a predictive model by using the remaining sample in the calibration set. The procedure was repeated with each sample left out in the calibration set. The RMSECV was calculated using the equation below (1).

$$\mathrm{RMSECV} = \sqrt{\frac{\sum_{i=1}^{n}\left(\hat{y}_{\setminus i} - y_i\right)^2}{n}} \quad (1)$$

where n is the number of samples in the calibration set, y_i is the reference measurement result for the sample i and $\hat{y}_i$ is estimated result of i th sample, when the model was built with eliminated sample i.

2.7. Software

Multivariate analysis was conducted by MATLAB Version 7.10.0 (Math Works, Natick, USA) under Windows 10. The PLS and GA- PLS algorithms were used in this work obtained by free downloaded from http://www.models.kvl.dk/.

3. Results and discussion

3.1. Fabrication and characterization of rGO-NS

Reduced graphene oxide gold nano-star nano-composites were prepared by seed-mediated growth method as highly

active SERS substrates through a two-step procedure shown schematic diagram 1. As discussed previously, rGO-NP (~10 nm diameter rGO embedded AuNP, see Fig. S1 in the Supporting Information for TEM images) was synthesized by the reduction of Au(III) complex ions using sodium citrate in the presence of graphene oxide. AuNP was formed in situ on the surface of GO, during stirring at ~85 °C, by the electrostatic interaction of positively charged gold (III) ion (Au^{+3}) and overall negatively charged surface of GO ascribed to a variety of oxygen-containing functional groups such as epoxy and hydroxyl groups on the basal plane as well as carbonyl and carboxyl groups along the edges [32,33]. The zeta potential values −36.1 mV with the concentration of 0.2 mg/mL indicated that the surface of GO is negatively charged due to above-stated oxygen-containing functional (Fig.S2), in addition, XRD pattern $2\theta = 11.0256^{\circ}$ also confirmed the above statement (Fig. 1b). Furthermore, FT-IR spectra of GO displayed several characteristic peaks associated with the oxygen-containing functional groups, including a broad peak at 3350 cm^{-1} is assignable to O–H stretching vibrations and the others peak at 1720 cm^{-1}, 1623 cm^{-1}, 1210 cm^{-1}, and 1073 cm^{-1} was caused by C=O stretching vibrations, unoxidized skeletal graphitic domains, C–OH stretching vibrations, and C–O stretching vibration, respectively [32,33]. Conversely, FT-IR spectra of rGO-NS exhibits the intensity of above oxygen-containing functional groups were declined, which also corroborates the reduction of GO (Fig. S3).

Subsequently, the seeds were allowed to grow into rGO-NS in the presence of additional $HAuCl_4$, HCl, $AgNO_3$ and AA as a reductant under stirring at 25 °C. The morphology of rGO-NS was confirmed by the low magnification TEM image. As seen in the TEM image, the average size of the AuNS is 60.37 nm with 8 branches (on average) (Fig. 1a). However, the XRD pattern $2\theta = 11.0256^{\circ}$ was disappeared when gold was embedded with GO and four new patterns appeared at $2\theta = 38.1601, 44.3585, 64.6998, 77.6722$ due to the decrease of the oxygen-containing functional group (Fig. 1b). These observations also confirmed the successful conjugation of rGO-NS.

In case of GO, two prominent peaks were found at 1324 cm^{-1} and 1595 cm^{-1}, which corresponds to the D and G band, in agreement with previous reports [15]. However, the intensity of D band and G band are ascribed to the defect of the oxygen-containing functional group and sp^2 hybridized carbon respectively [34]. For rGO-NS nano-composite, the D and G bands were also observed, but the intensity ratio of the D and G bands which means I_D/I_G was apparently increased in contrast with the GO at the same experimental conditions. Where the value of I_D/I_G ratio was 0.97 and 1.23 for GO and rGO-NS respectively, which indicated the reduction of GO [35] as well as the accession of novel metal nanostructure with GO, also increase the LSPR of the D and G bands based on EM enhancement of SERS [36] (Fig. 1c).

The morphology of GO, rGO-NP and rGO-NS nano-composite were examined by the SEM image. The SEM image of the pure GO sheet revealed that the surface of the sheet is translucent and shrivelled with some folds (Fig. 1d). In fact, the SEM image of rGO-NS exhibits the nano-composites were agglomerated (Fig. S4), which was also indicated that lower density of oxygen functional groups influences the growth of gold nano-star agglomerates, in agreements with previous reports [32]. The chemical composition of rGO-NS was determined by EDS analysis. The signals of gold, carbon and oxygen were found by EDS analysis, which demonstrated that graphene and gold were the compositions of rGO-NS (Fig. S5).

The GO, rGO, rGO-NP and rGO-NS were confirmed by UV–vis spectroscopy (Fig. 1e). When GO was partially reduced, the band around 300 nm disappeared due to the recovery of the electronic conjugated structure after reduction as the absorption increases in the UV–vis region [20]. However, Au nano-composite showed a typical band around 520 nm in the visible spectrum region due to the localized surface plasmon resonance (LSPR) [32]. Moreover, the LSPR spectra showed red-shifted LSPR bands with a shoulder around 700 nm after the formation of rGO-NS.

To investigate the Raman scattering and SERS effect, 12 μg/mL of rGO, rGO-NP and rGO-NS were used as SERS substrate for sensing CV with the concentration of 2 μM as Raman probe molecule under the same experimental condition. Fig. S6 showed the SERS spectra of CV with rGO-NS nano-composites which were better than the rGO and rGO-NP. Analytical enhancement factors (AEFs) of the rGO, rGO-NP and rGO-NS were calculated using the procedure and formula given by Ru et al., 2006 [37].

$$AEF = \frac{I_{SERS}/C_{SERS}}{I_{RS}/C_{RS}}$$

Where CRS is the concentrations of an analyte and IRS is the Raman signal intensities produced by that analyte under non-SERS conditions. CSERS and ISERS are the concentrations of analyte absorbed on a SERS-active substrate and its corresponding SERS signal intensities respectively. Calculated result of AEF for rGO, rGO-NP and rGO-NS are captured in Table S1 and rGO-NS gave the highest AEF of 2.34 × 106 compared to rGO and rGO-NP. This thus formed the basis for the synthesis and application of rGO-NS as a substrate for the detection as opposed to the others. In addition, to reveal the SERS ability of the rGO-NS nano-composite, as shown in Fig. S7, SERS spectra of CV solution with different concentrations (0.1, 1, 2, 5, 10, 50 and 100 μM) were measured by using the rGO-NS nano-composite as substrates. The SERS signal intensity decreases with decreasing concentration of the CV but it is still detectable even at the concentration of 1 μM under the same experimental condition.

3.2. *SERS detection strategy of AC*

The AC residue was analyzed with the proposed sensor using rGO-NS nano-composite as a SERS substrate, as previously discussed. rGO-NS nano-composite may combine with AC electro-statically. The different concentration of AC gave rise to the plasmonic coupling with the rGO-NS which yielded a strong SERS signal. A linear relationship was observed between the concentration of AC from 1.0×10^{-4} to 1.0×10^{3} μg/mL and the SERS intensity. The SERS intensity increased with increasing concentration of AC. AC gave the highest peak at 634 cm^{-1}, which can be ascribed to the ring structure of the molecule [16] and the 443 cm^{-1}, 549 cm^{-1}, 825 cm^{-1} and 1107 cm^{-1} peak were assignable to C–N–C bond, C–C bond, C–N bond and ring breathing vibrational mode respectively

[38]. The others peaks also were observed at 576 cm^{-1}, 908 cm^{-1}, 1039 cm^{-1}, 1218 cm^{-1}, 1415 cm^{-1}, 1490 cm^{-1}, 1583 cm^{-1}. 3D structure of AC was shown in Fig. S8. Raman peak for AC as shown in Fig. 2a and Fig. 2b illustrates the typical SERS intensity and fingerprint pattern for the detection of various concentrations of AC residue in green tea using the proposed method.

3.3. *Quantitative analysis with chemometrics model*

Prior to modeling, different concentrations (blank, 0.00001, 0.0001, 0.001, 0.01, 0.1, 1, 10, 100 and 1000 μg/mL) of AC samples were prepared and analyzed as described by Ru-Yan et al., 2013 to fix the range of detection and collected spectra were used to build a chemometric model. It was observed that when the concentration of AC was less than 0.0001 μg/mL no Raman signal was generated (Fig. 2b). The detection range of AC was selected from 1.0×10^{-4} to 1.0×10^{3} μg/mL using the developed method, for the different concentrations of AC samples. The spectra of one hundred and sixty samples with concentrations 0.0001, 0.001, 0.01, 0.1, 1, 10, 100 and 1000 μg/mL were selected (Fig. S9a) then preprocessing was conducted by SNV (Fig. S9b) and divided them into two subsets to build the chemometric model. The first subset is called calibration or training set, which was used to build the model and the prediction or test set which was used to check the robustness of the model. To avoid bias, all samples were arranged according to their respective y-value (viz. the reference value of AC). According to 3/2 division of calibration/prediction spectra, two spectra for every five samples were selected into the prediction set, so that finally the prediction set contains 64 spectra and the remaining 96 spectra constitute the calibration set.

First, PLS algorithm was applied to build a model, as the number of principal components is a crucial parameter to calibrate a model. The optimal number of PCs 8 was selected from the lowest value of RMSECV (Fig. 3c). The values of RMSECV, Rc, RMSEP, and Rp were 0.87, 0.9289, 0.796, 0.9367 respectively in the calibration and prediction set. According to the result of PLS, the R value of calibration set is lower than the prediction set and RMSECV value was higher than RMSECP, indicates the presence of irrelevant variable other than target variable, which ultimately leads to a reduction in the predictability of the model. Fig. 3a and b showed the scatter plot for both calibration and prediction set making it necessary to implement another algorithm to build a calibration model.

GA analysis was applied to select the variables whereas PLS was used to build the model. Fig. 3f shows the bar chart of the cumulative frequency selected for each variable after hundred runs of GA from SNV pretreated spectral data for predicting AC residue in green tea and red dashed line indicated that frequency of variables was selected above 3. Finally, 85 spectral variables were selected from 874 full spectral variables for GA-PLS modeling, among the 85 variables the number 129 variables corresponded to the peak 634 cm^{-1}; variables 39 and 40, 92 and 93, 102 and 104, 209 and 210, 251 and 254, 348 and 349, 555 and 556 corresponded to the peaks 443 cm^{-1}, 549 cm^{-1}, 576 cm^{-1}, 825 cm^{-1}, 908 cm^{-1}, 1107 cm^{-1}, 1490 cm^{-1} respectively. Additionally, variables 319, 407, 515 and 608 were related to the peaks 1039 cm^{-1}, 1218 cm^{-1}, 1415 cm^{-1} and 1583 cm^{-1} respectively. Finally, the GA-PLS model was established with 6 PCs (Fig. S10). The optimal number of PCs 6 was determined by the lowest value of RMCECV. Here, the value of RMSECV was 0.386 and Rc was 0.9772 in the calibration set as well as RMSEP was 0.479 and Rp was 0.9757 in the prediction set. Fig. 3d and e showed the scatter plot of a correlation between the reference value of AC and SERS predicted value in the calibration and prediction sets respectively. Table 1 shows the summary result of PLS and GA-PLS. In the GA-PLS model, the value of Rc was higher than Rp and the lowest value of RMSEC and RMSEP which leads the higher prediction accuracy of the model. This result indicates that the GA-PLS calibration could serve as a reliable prediction model to predict the concentration of AC residue in green tea.

3.4. *Accuracy and precision of the developed sensor*

In order to demonstrate the reliability of the proposed sensor, known concentrations of AC were added to real tea sample for the recovery evaluation to confirm the applicability of the developed SERS sensor. The accuracy and precision were evaluated by spiking green tea (Longjing tea leaves) sample with a known concentration of AC ranging from 1.0×10^{-4} to 1.0×10^{3} μg/mL. The predicted concentration of AC was determined by the established GA-PLS model. For recovery and RSD calculation, each gradient concentration of AC sample was prepared ten times for the acquisition of SERS

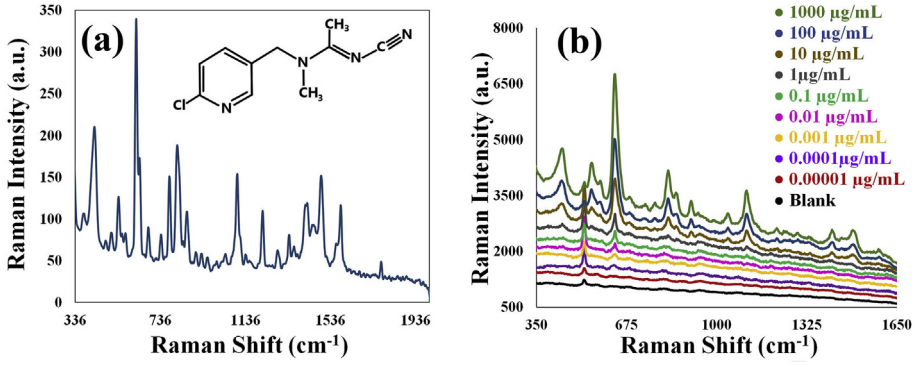

Fig. 2 – Normal Raman spectrum of AC (a). SERS spectra of AC with various concentrations (blank, 0.00001, 0.0001, 0.001, 0.01, 0.1, 1, 10, 100 and 1000 μg/mL) adsorbed on rGO-NS nano-composite (b).

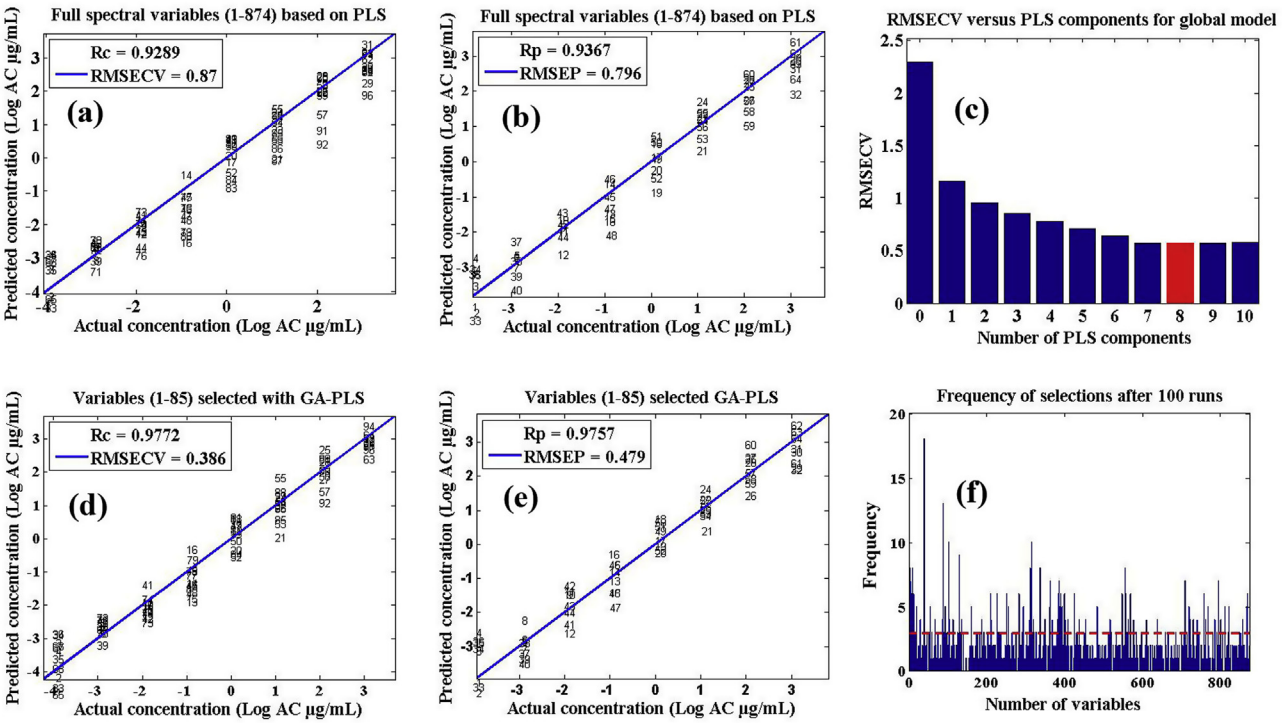

Fig. 3 – Scatter plot of predicted concentration (log AC μg/mL) vs. actual concentration (log AC μg/mL) in calibration set (a) and prediction set (b) using the PLS model. Optimum principal component for PLS model (c). Predicted concentration (log AC μg/mL) vs. actual concentration (log AC μg/mL) in calibration set (c) and prediction set (d) using the GA-PLS model. Cumulative frequencies for spectra variables selected by GA (f).

Table 1 – Model performance results for the chemometric algorithms for AC residue quantification in green tea.

Chemometric algorithms	Optimum PCs	Calibration set		Prediction set	
		Rc	RMSECV (log AC μg/mL)	Rp	RMSEP (log AC μg/mL)
PLS	8	0.9289	0.87	0.9367	0.796
GA-PLS	**6**	**0.9772**	**0.386**	**0.9757**	**0.479**

Bold indicates GA-PLS algorithm achieved optimum results.

Table 2 – Determination of AC residue in green tea by the proposed method.

Sample	Spiked concentration (μg/mL)	Detection value (μg/mL) (Mean[a] ± SD[b])	Recovery (%)	RSD (%)
Green tea	0.0001	0.000116 ± 0.00001	115.88	5.98
	0.001	0.001149 ± 0.0001	114.89	5.74
	0.01	0.01108 ± 0.0006	110.98	5.86
	0.1	0.1037 ± 0.0051	103.90	4.88
	1	1.077 ± 0.0644	108.90	5.91
	10	9.833 ± 0.1467	98.43	1.49
	100	99.281 ± 0.1507	99.28	0.15
	1000	970.38 ± 0.4301	97.06	0.04

[a] Mean, average value of ten tests.
[b] SD, standard deviation (n = 10).

spectrum. The proposed sensor achieved the recovery varied from 97.06% to 115.88% with RSD lower than 5.98% (Table 2) and a LOD of 2.13×10^{-5} μg/mL (S/N = 3), which indicates that the developed sensor combined with GA-PLS model has high accuracy and precision to detect AC residue in green tea. For reproducibility, three different concentration of 0.0001, 1 and 1000 μg/mL were selected and analyzed five consecutive days according to the procedure of recovery test. The proposed

Table 3 – Comparison of the linear ranges and LODs of this method and other reported methods for AC detection.

Method	sample	Linear range (μg/mL)	LOD (μg/mL)	Reference
HPLC	Fruit	1×10^{-4}–1	2.5×10^{-4}	[5]
LC-MS-MS	butterbur	$4 \times 10^{-3} - 0.4$	6.0×10^{-4}	[6]
ELISA	Vegetables and fruits	$3 \times 10^{-4} - 1.25 \times 10^{-2}$	1.0×10^{-3}	[7]
Fluorescent	Vegetables	$1.11 \times 10^{-2} - 2.23 \times 10^{-1}$	1.6×10^{-3}	[8]
SERS	Apple	$1.2 \times 10^{-3} - 15.31$	5.4×10^{-3}	[9]
SERS based rGO-NS sensor	**Green tea**	**1.0×10^{-4}–1.0×10^{3}**	**2.13×10^{-5}**	**This work**

sensor calculated RSD was lower than 6% as seen in Table S2, which confirms the results achieved using rGO-NS coupled GA-PLS model as highly reproducible and reliable of predicting AC residue in green tea. As well as Table 3 summarizes the comparative analytical performance for AC residue detection in the linear range and LOD among the proposed method and other recently reported literature, which suggests that the proposed label-free, simple and highly sensitive rGO-NS SERS based nanosensor coupled to GA-PLS has a relatively low LOD compared with those of other recently reported methods.

4. Conclusion

The overall result indicates that SERS coupled with the seed-mediated growth of reduced graphene oxide supported gold nano-star nano-composite based on GA-PLS model has high potential to quantify AC residue in green tea with a high degree of accuracy. Additionally, the calibration model of GA-PLS for AC achieved a good correlation coefficient Rp of 0.9757 and RMSEP of 0.479 in prediction set. A good correlation between AC concentration and SERS intensity yielding from rGO-NS nanosensor was found to be linear from 1.0×10^{-4} to 1.0×10^{3} μg/mL with LOD of 2.13×10^{-5} μg/mL. Furthermore, the accuracy and precision tests showed satisfactory results with RSD lower than 5.98%. The developed SERS based rGO-NS nano-composite nanosensor could be employed as a label-free, simple, sensitive, rapid, efficient and stable platform to detect multi-pesticides in green tea.

Conflicts of interest

The authors of the manuscript declare that there is no conflict of interest regarding the publication of this study.

Acknowledgement

This work has been financially supported by the National Natural Science Foundation of China (31772063), National Key R&D Program of China (2016YFD0401205), and Key R&D Program of Jiangsu Province (BE2017357 and BE2015308).

Appendix A. Supplementary data

Supplementary data related to this article can be found at https://doi.org/10.1016/j.jfda.2018.06.004.

REFERENCES

[1] Fu C, Liu J, Luan R, Chen K, Wang H. Tea consumption and health beneficences of green 2 tea drinking-A community-based cross-sectional 3 study in urban Chinese men 4. Methodology 2013;56:57.
[2] Werba JP, Misaka S, Giroli MG, Shimomura K, Amato M, Simonelli N, et al. Update of green tea interactions with cardiovascular drugs and putative mechanisms. J Food Drug Anal 2018:S72–7.
[3] Chen M, Tao L, McLean J, Lu C. Quantitative analysis of neonicotinoid insecticide residues in foods: implication for dietary exposures. J Agric Food Chem 2014;62:6082–90.
[4] Cimino AM, Boyles AL, Thayer KA, Perry MJ. Effects of neonicotinoid pesticide exposure on human health: a systematic review. Environ Health Perspect 2017;125:155.
[5] Vichapong J, Burakham R, Srijaranai S. Alternative liquid–liquid microextraction as cleanup for determination of neonicotinoid pesticides prior HPLC analysis. Chromatographia 2016;79:285–91.
[6] Lee HS, Kim S-W, El-Aty AA, Chung HS, Kabir MH, Rahman MM, et al. Liquid chromatography–tandem mass spectrometry quantification of acetamiprid and thiacloprid residues in butterbur grown under regulated conditions. J Chromatogr B 2017;1055:172–7.
[7] Watanabe E, Miyake S, Yogo Y. Review of enzyme-linked immunosorbent assays (ELISAs) for analyses of neonicotinoid insecticides in agro-environments. J Agric Food Chem 2013;61:12459–72.
[8] Guo J, Li Y, Wang L, Xu J, Huang Y, Luo Y, et al. Aptamer-based fluorescent screening assay for acetamiprid via inner filter effect of gold nanoparticles on the fluorescence of CdTe quantum dots. Anal Bioanal Chem 2016;408:557–66.
[9] Zhai C, Peng Y, Li Y, Chao K. Extraction and identification of mixed pesticides' Raman signal and establishment of their prediction models. J Raman Spectrosc 2017;48:494–500.
[10] Li H, Chen Q, Hassan MM, Ouyang Q, Jiao T, Xu Y, et al. AuNS@ Ag core-shell nanocubes grafted with rhodamine for concurrent metal-enhanced fluorescence and surfaced enhanced Raman determination of mercury ions. Anal Chim Acta 2018:94–103.
[11] Yang M, Liu G, Mehedi HM, Ouyang Q, Chen Q. A universal sers aptasensor based on DTNB labeled GNTs/Ag core-shell nanotriangle and CS-Fe3O4 magnetic-bead trace detection of Aflatoxin B1. Anal Chim Acta 2017;986:122–30.
[12] Li H, Chen Q, Hassan MM, Chen X, Ouyang Q, Guo Z, et al. A magnetite/PMAA nanospheres-targeting SERS aptasensor for tetracycline sensing using mercapto molecules embedded core/shell nanoparticles for signal amplification. Biosens Bioelectron 2017;92:192–9.
[13] Wang L, Xu X-M, Chen Y-S, Ren J, Liu Y-T. HPTLC-FLD-SERS as a facile and reliable screening tool: exemplarily shown with tyramine in cheese. J Food Drug Anal 2018;26(2):688–95.
[14] Xie X, Gao G, Kang S, Lei Y, Pan Z, Shibayama T, et al. Toward hybrid Au nanorods@ M (Au, Ag, Pd and Pt) core–shell

heterostructures for ultrasensitive SERS probes. Nanotechnology 2017;28:245602.
[15] Zheng H, Ni D, Yu Z, Liang P. Preparation of SERS-active substrates based on graphene oxide/silver nanocomposites for rapid zdetection of l-Theanine. Food Chem 2017;217:511–6.
[16] Zhang H, Kang Y, Liu P, Tao X, Pei J, Li H, et al. Determination of pesticides by surface-enhanced Raman spectroscopy on gold-nanoparticle-modified polymethacrylate. Anal Lett 2016;49:2268–78.
[17] Su Q, Ma X, Dong J, Jiang C, Qian W. A reproducible SERS substrate based on electrostatically assisted APTES-functionalized surface-assembly of gold nanostars. ACS Appl Mater Interfaces 2011;3:1873–9.
[18] Novoselov KS, Geim AK, Morozov SV, Jiang D, Zhang Y, Dubonos SV, et al. Electric field effect in atomically thin carbon films. Science 2004;306:666–9.
[19] Kavitha C, Bramhaiah K, John NS, Ramachandran B. Low cost, ultra-thin films of reduced graphene oxide–Ag nanoparticle hybrids as SERS based excellent dye sensors. Chem Phys Lett 2015;629:81–6.
[20] Wang Y, Polavarapu L, Liz-Marzán LM. Reduced graphene oxide-supported gold nanostars for improved SERS sensing and drug delivery. ACS Appl Mater Interfaces 2014;6:21798–805.
[21] Janči T, Valinger D, Kljusurić JG, Mikac L, Vidaček S, Ivanda M. Determination of histamine in fish by Surface Enhanced Raman Spectroscopy using silver colloid SERS substrates. Food Chem 2017;224:48–54.
[22] Sun L-L, Wang M, Zhang H-J, Liu Y-N, Ren X-L, Deng Y-R, et al. Comprehensive analysis of Polygoni Multiflori Radix of different geographical origins using ultra-high-performance liquid chromatography fingerprints and multivariate chemometric methods. J Food Drug Anal 2016:90–9.
[23] Lim DK, Mo C, Lee JH, Long NP, Dong Z, Li J, et al. The integration of multi-platform MS-based metabolomics and multivariate analysis for the geographical origin discrimination of Oryza sativa L. J Food Drug Anal 2017 :769–77.
[24] Kutsanedzie FY, Hao L, Yan S, Ouyang Q, Chen Q. Near infrared chemo-responsive dye intermediaries spectra-based in-situ quantification of volatile organic compounds. Sensor Actuator B Chem 2018;254:597–602.
[25] Chen Q, Hu W, Su J, Li H, Ouyang Q, Zhao J. Nondestructively sensing of total viable count (TVC) in chicken using an artificial olfaction system based colorimetric sensor array. J Food Eng 2016;168:259–66.
[26] Hu W, He R, Hou F, Ouyang Q, Chen Q. Real-time monitoring of alcalase hydrolysis of egg white protein using near infrared spectroscopy technique combined with efficient modeling algorithm. Int J Food Prop 2017;20:1488–99.
[27] Kutsanedzie FY, Chen Q, Hassan MM, Yang M, Sun H, Rahman MH. Near infrared system coupled chemometric algorithms for enumeration of total fungi count in cocoa beans neat solution. Food Chem 2018;240:231–8.
[28] Khulal U, Zhao J, Hu W, Chen Q. Nondestructive quantifying total volatile basic nitrogen (TVB-N) content in chicken using hyperspectral imaging (HSI) technique combined with different data dimension reduction algorithms. Food Chem 2016;197:1191–9.
[29] Li H, Chen Q, Zhao J, Wu M. Nondestructive detection of total volatile basic nitrogen (TVB-N) content in pork meat by integrating hyperspectral imaging and colorimetric sensor combined with a nonlinear data fusion. LWT Food Sci Technol 2015;63:268–74.
[30] Zareef M, Chen Q, Ouyang Q, Kutsanedzie F, Hassan MM, Annavaram V, et al. Prediction of amino acids, caffeine, theaflavins and water extract in black tea by FT-NIR spectroscopy coupled chemometrics algorithms. Anal Meth 2018:3023–31.
[31] Huang L, Zhao J, Chen Q, Zhang Y. Rapid detection of total viable count (TVC) in pork meat by hyperspectral imaging. Food Res Int 2013;54:821–8.
[32] Goncalves G, Marques PA, Granadeiro CM, Nogueira HI, Singh M, Gracio J. Surface modification of graphene nanosheets with gold nanoparticles: the role of oxygen moieties at graphene surface on gold nucleation and growth. Chem Mater 2009;21:4796–802.
[33] Salehi Z, Kianpour B, Ebrahimi A, Fatemi S. Evaluating the effect of graphite source and operating conditions on the synthesis of graphene oxide. Journal Chem Petrol Eng 2017;50:37–45.
[34] Park Y, Soon Choi K, Young Kim S. Graphene oxide/PEDOT: PSS and reduced graphene oxide/PEDOT: PSS hole extraction layers in organic photovoltaic cells. physica status solidi (a) 2012;209:1363–8.
[35] Ko YC, Fang HY, Chen DH. Fabrication of Ag/ZnO/reduced graphene oxide nanocomposite for SERS detection and multiway killing of bacteria. J Alloy Comp 2017;695:1145–53.
[36] Rajab M, Mougin K, Derivaz M, Josien L, Luchnikov V, Toufaily J, et al. Controlling shape and spatial organization of silver crystals by site-selective chemical growth method for improving surface enhanced Raman scattering activity. Colloid Surface Physicochem Eng Aspect 2015;484:508–17.
[37] Le Ru E, Blackie E, Meyer M, Etchegoin PG. Surface enhanced Raman scattering enhancement factors: a comprehensive study. J Phys Chem C 2007;111:13794–803.
[38] Zhai C, Li Y, Peng Y, Xu T, Dhakal S, editors. Detection of acetamiprid in fruits by surface enhanced Raman spectroscopy. 2015 ASABE annual international meeting. American Society of Agricultural and Biological Engineers; 2015.